ACCOUNTS
of chemical research

Enhancing Pseudocapacitive Charge Storage in Polymer Templated Mesoporous Materials

IRIS E. RAUDA,[†,∥] VERONICA AUGUSTYN,[‡,∥] BRUCE DUNN,[*,‡,§] AND SARAH H. TOLBERT[*,†,§]

[†]*Department of Chemistry and Biochemistry, UCLA, Los Angeles, California 90095-1569, United States,* [‡]*Department of Materials Science and Engineering, UCLA, Los Angeles, California 90095-1595, United States, and* [§]*The California NanoSystems Institute (CNSI), UCLA, Los Angeles, California 90095-7227, United States*

RECEIVED ON JUNE 1, 2012

CONSPECTUS

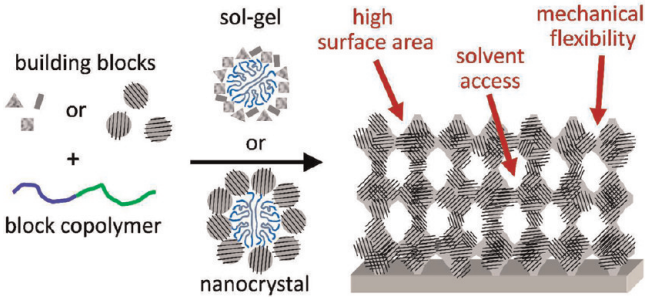

Growing global energy demands coupled with environmental concerns have increased the need for renewable energy sources. For intermittent renewable sources like solar and wind to become available on demand will require the use of energy storage devices. Batteries and supercapacitors, also known as electrochemical capacitors (ECs), represent the most widely used energy storage devices. Supercapacitors are frequently overlooked as an energy storage technology, however, despite the fact that these devices provide greater power, much faster response times, and longer cycle life than batteries. Their limitation is that the energy density of ECs is significantly lower than that of batteries, and this has limited their potential applications.

This Account reviews our recent work on improving pseudocapacitive energy storage performance by tailoring the electrode architecture. We report our studies of mesoporous transition metal oxide architectures that store charge through surface or near-surface redox reactions, a phenomenon termed pseudocapacitance. The faradaic nature of pseudocapacitance leads to significant increases in energy density and thus represents an exciting future direction for ECs. We show that both the choice of material and electrode architecture is important for producing the ideal pseudocapacitor device.

Here we first briefly review the current state of electrode architectures for pseudocapacitors, from slurry electrodes to carbon/metal oxide composites. We then describe the synthesis of mesoporous films made with amphiphilic diblock copolymer templating agents, specifically those optimized for pseudocapacitive charge storage. These include films synthesized from nanoparticle building blocks and films made from traditional battery materials. In the case of more traditional battery materials, we focus on using flexible architectures to minimize the strain associated with lithium intercalation, that is, the accumulation of lithium ions or atoms between the layers of cathode or anode materials that occurs as batteries charge and discharge. Electrochemical analysis of these mesoporous films allows for a detailed understanding of the origin of charge storage by separating capacitive contributions from traditional diffusion-controlled intercalation processes. We also discuss methods to separate the two contributions to capacitance: double-layer capacitance and pseudocapacitance. Understanding these contributions should allow the selection of materials with an optimized architecture that maximize the contribution from pseudocapacitance.

From our studies, we show that nanocrystal-based nanoporous materials offer an architecture optimized for high levels of redox or surface pseudocapacitance. Interestingly, in some cases, materials engineered to minimize the strain associated with lithium insertion can also show intercalation pseudocapacitance, which is a process where insertion processes become so kinetically facile that they appear capacitive.

Finally, we conclude with a summary of simple design rules that should result in high-power, high-energy-density electrode architectures. These design rules include assembling small, nanosized building blocks to maximize electrode surface area; maintaining an interconnected, open mesoporosity to facilitate solvent diffusion; seeking flexibility in electrode structure to facilitate volume expansion during lithium insertion; optimizing crystalline domain size and orientation; and creating effective electron transport pathways.

Published on the Web 03/13/2013 www.pubs.acs.org/accounts
10.1021/ar300167h

1. Introduction

The projected doubling of worldwide energy consumption over the next 50 years presents one of the great scientific, technological, and environmental challenges of our times.[1] This predicament has brought increased awareness of the need for a sustainable energy future based on renewable sources. In order to realize the large-scale solar or wind-based electrical generation projects that will be critical to meeting future energy demands, new electrical energy storage (EES) systems must also be developed to supply energy continuously.

The leading EES technologies today are batteries and electrochemical capacitors (ECs). Both are electrochemical systems and the power and energy relationship between them is shown in a Ragone Plot (Figure 1a).[2] The success of lithium-ion batteries in consumer electronics and the first generation of plug-in hybrids has led to significant advances. Nonetheless, it is evident that ECs possess a number of very attractive properties that complement or exceed the capabilities of batteries: fast charging within seconds, cycle life in excess of 500 000 cycles, and the ability to deliver >10× more power.[3] As a result, there are areas where ECs can find unique applications. For example, the fast charging properties of ECs are needed for regenerative braking in light rail, frequency regulation in smart grids, and they are well-suited for storing the intermittent energy profiles of renewable energy sources.[3] Limiting the widespread use of ECs is their energy density: current commercial devices store less than 10 $Wh \cdot kg^{-1}$,[1] while state of the art asymmetric EC devices achieve ~30 $Wh \cdot kg^{-1}$.[4]

Based on their energy storage mechanisms, ECs can be divided into two categories (Figure 1b): electric double-layer capacitors (EDLCs) and pseudocapacitors. EDLCs store charge in a thin double-layer located at the interface between the electrolyte and the electrode. This type of capacitance (C) occurs on every electrode surface and is dependent upon the surface area of the electrode:

$$C = \frac{\varepsilon S}{d}$$

where ε is the relative permittivity, S is the surface area, and d is the thickness of the double-layer. Since d is small (just a few angstroms, depending on electrolyte ion and solvent dimensions),[5] capacitances exhibited by EDLCs are much higher than those of traditional dielectric capacitors. Carbon-based materials are used as EDLC electrodes because of their high surface area and electronic conductivity, and capacitance values of 100−150 $F \cdot g^{-1}$ are achieved in some materials.[6] In an ideal capacitor, the current is independent of potential and therefore a cyclic voltammogram (CV) will exhibit rectangular ("mirror") behavior. In an EDLC, the adsorption of ions on the surface results in mostly rectangular CVs, although some potential dependence can occur through overscreening and crowding at the double-layer.[7]

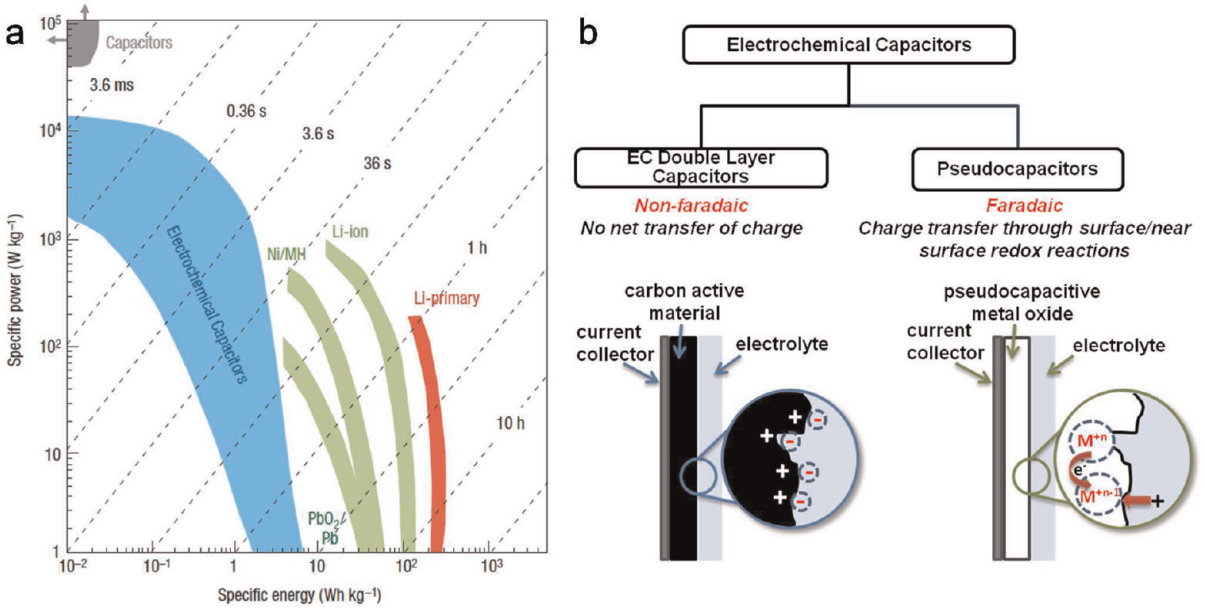

FIGURE 1. (a) Power vs energy density graph (Ragone Plot) of energy storage devices (Adapted from ref 2. Copyright Nature 2008). (b) Mechanisms for capacitive charge storage at an electrode surface.

Pseudocapacitance is a faradaic process that involves surface or near-surface redox reactions. The interest in utilizing pseudocapacitance arises because the energy density associated with faradaic reactions is at least 10× greater than that of double-layer processes: above 100 $\mu F \cdot cm^{-2}$ for pseudocapacitance versus 10 $\mu F \cdot cm^{-2}$ for EDLCs.[8] Traditionally, most pseudocapacitive materials are transition metal oxides, whose specific capacitance values exceed 1000 $F \cdot g^{-1}$. Pseudocapacitance often exhibits a dependence on potential because it involves redox reactions, which can lead to peaks in the CVs.

Over the past few years, we have used soft-templating of transition metal oxides to create mesoporous films that provide a novel architecture for high-quality pseudocapacitor materials.[9−13] Our materials contain a number of features that are beneficial for pseudocapacitive charge storage reactions: high surface area, homogeneous porosity, nanosized crystalline domains, and iso-orientation. The mesoporous morphologies enable electrolyte access to the redox-active walls and enhanced kinetics due to the relatively short diffusion paths for electrons and ions. In this Account, we describe the current understanding of surface redox reactions for charge storage, how porous electrode architectures have been used in ECs, analysis techniques to determine surface charge storage, and how mesoporous electrode architectures can enhance this behavior.

The origin of pseudocapacitance was described thoroughly by Conway.[5] In this description, pseudocapacitance occurs whenever the amount of charge storage (Q) depends on the change in potential (ΔV), giving the form of a capacitance ($Q/\Delta V$). Based on this theory, we identify three faradaic charge storage processes that can occur when a redox-active oxide is immersed in electrolyte. (1) Ions intercalate into preferred crystallographic sites, often in materials characterized by layered or tunnel structures. The intercalation is accompanied by metal valence change to preserve electrical neutrality. (2) Ions are electrochemically adsorbed onto the surface of the material. In this mechanism, referred to as redox pseudocapacitance, adsorption is associated with a change in the metal valence state. This process is kinetically facile because of the short-range nature of ion transport. (3) In our research, we have also observed mesoporous oxides in which the intercalation is facile, giving rise to a capacitive response. This third process is referred to as intercalation pseudocapacitance.

In intercalation pseudocapacitance, the material's behavior is sometimes described as "transitional" between batteries and ECs because while the ion insertion may be facile, bulk solid-state diffusion still leads to slow processes.[5] Widely used intercalation materials such as $LiCoO_2$ show charging time of over 1 h, which is substantially beneath the EC power density regime. However, in nanostructured materials such as mesoporous films, diffusion distances are drastically decreased from the bulk and intercalation can kinetically behave in a more capacitive manner. In this class of materials, the distinction between capacitive and diffusive mechanisms is particularly important. We will elaborate later on such analysis techniques.

2. Architectures for Fast Energy Storage

It is now well established that controlling the architecture of electrode materials plays a pivotal role in enhancing the performance of EES devices. As discussed above, the reactions that govern charge storage in pseudocapacitive materials are dependent on a combination of fast electron- and ion-transfer to the active sites. Consequently, there has been a push to use nanostructured materials to create porosity and increase surface area. The combination of high surface area and nanoscale dimensions allows for short diffusion lengths and easy access to surface redox sites. Porosity is needed for solvent diffusion, and the pore size can have a significant influence on the capacitance.[6] Small domain sizes can also lead to suppression of phase transitions and reduced intercalation stress.[14]

2.1. Slurry-Cast Electrodes. The traditional method for fabricating EC electrodes involves casting an electrode from a slurry containing active material, conductive additive, and binder. This approach enables electrodes to be made from virtually any powdered material. Electrodes have been produced from transition metal oxides in the form of nanoplates, nanorods, and nanoparticles, as well as powders of mesoporous materials.[15] In many cases, these mesoporous powders are made using hard templates such as opals or surfactant-templated silica.[16] The versatility of hard-templating is demonstrated by the wide range of materials that can be prepared including β-MnO_2, $Li_4Ti_5O_{12}$, and $LiCoO_2$.[17] The disadvantage is the multistep processing.

One of the principal disadvantages of slurry-cast electrodes is that they tend to bury the surface of the active material,[18] limiting electrolyte access to surface-redox sites and leading to poor rate capabilities. In addition, a significant percentage of the electrode (>15 wt %) is made up of inactive materials. Moreover, slurry-electrodes may contain large interparticle distances that lead to low active material densities. It can also be difficult to deconvolute the

electrochemical properties of the active material from the electrochemical response of the electrode.

2.2. Nanomaterials on Conductive Scaffolds. There are many examples of composites that utilize a nanostructured version of a good electronic conductor that is coated with a transition metal oxide. One example utilizes porous metal foams coated with transition metal oxides.[19] A more popular approach uses high surface area carbons as the scaffold, including carbon nanotubes, graphene, or fibers.[20] For most of these composites, fast charge/discharge kinetics are observed because a highly conductive network exists throughout the electrode. However, both volumetric and gravimetric capacitances are greatly decreased when the mass of the inactive conductive scaffold is considered.[21]

2.3. Thin-Film Electrodes. Another approach is to deposit a thin-film of active material onto a conductive substrate, such as a metal foil or tin-doped indium oxide (ITO)-coated glass. Films can be deposited by a variety of solution-phase methods including drop-casting, dipping, and electrodeposition.[22] Since no conductive additives or binders are used, the electrochemical properties of thin-films can generally be unequivocally assigned to the active material, making these systems particularly useful for fundamental studies. Also, if the films are thin, the capacitance and rate capabilities can be high as problems with electrical conductivity are minimized. Of course, the drawback is that the total energy storage of such electrodes is small.

Mesoporous architectures can be directly produced as thin-film electrodes using soft-templating. Here, we focus on materials made using amphiphilic templates, including ionic and nonionic surfactants, small triblock copolymers (specifically the pluronic family of polymers) and more recently, a growing family of larger diblock copolymers (DBCP) that readily form micelles in solution and self-organize into hexagonal or cubic structures via an evaporation-induced self-assembly (EISA) process.[23−25] Casting a solution of template and inorganic precursor onto a substrate results in an inorganic−organic composite. The template can be subsequently removed to produce a mesoporous inorganic material. While there are numerous reports of metal oxide films produced using EISA methods, the challenge for electrode materials is that crystalline oxides are generally needed. When small surfactants or pluronics are used, the materials are often amorphous because the pore walls are too thin to crystallize without destroying the nanoscale architecture. In the next section, we demonstrate that large DBCP can circumvent this problem by producing thicker pore walls that effectively allow for crystallization of virtually any material. Such polymers also allow larger building blocks, such as preformed nanocrystals, to be organized into porous networks.

SCHEME 1. Evaporation-Induced Self-Assembly Process for Producing Cubic Mesoporous Films[a]

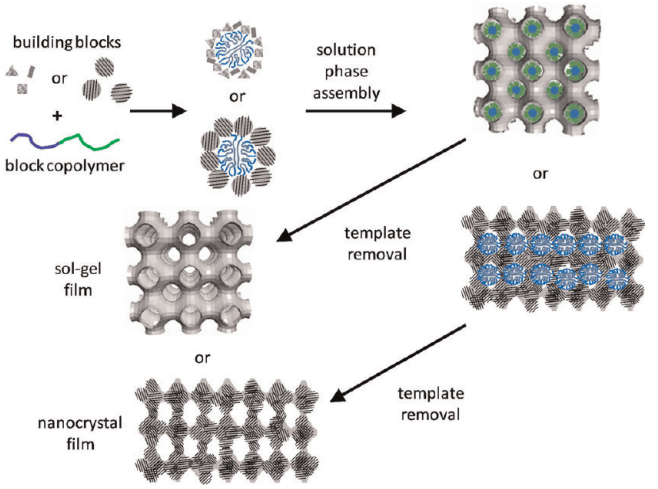

[a]The building blocks can be either molecular precursors leading to sol-gel-based films, or pre-formed nanocrystals, leading to nanocrystal-based films.

3. Synthesis of Mesoporous Films

In order to examine applications of mesoporous films for pseudocapacitive charge storage, we must first review synthetic methods used to make these materials. The general method is depicted in Scheme 1. In this process, inorganic building blocks coassemble with an amphiphilic DBCP using EISA. Sol−gel chemistries are well suited for such polymer-templating techniques. In a typical synthesis, inorganic precursors, often metal alkoxides or metal salts, are dissolved in polar media along with the DBCP to form the *sol*. Sols generally contain some water plus a more volatile organic solvent such as methanol. When the solution is cast onto a substrate, either through dip-coating, spin-coating, or drop-casting, the volatile solvent evaporates and the solution becomes enriched in water, causing any free DBCP to form micelles. The micelles then coassemble with the inorganic precursors into cubic or hexagonal structures as the inorganic precursors undergo hydrolysis and condensation reactions.[23−26] The dry film can be thermally treated to decompose the polymer template and further condense/crystallize the inorganic framework, leaving behind the desired mesoporous film.

Figure 2a,b shows scanning electron microscope (SEM) and transmission electron microscope (TEM) images of a sol−gel derived nanoporous Nb_2O_5 film that was

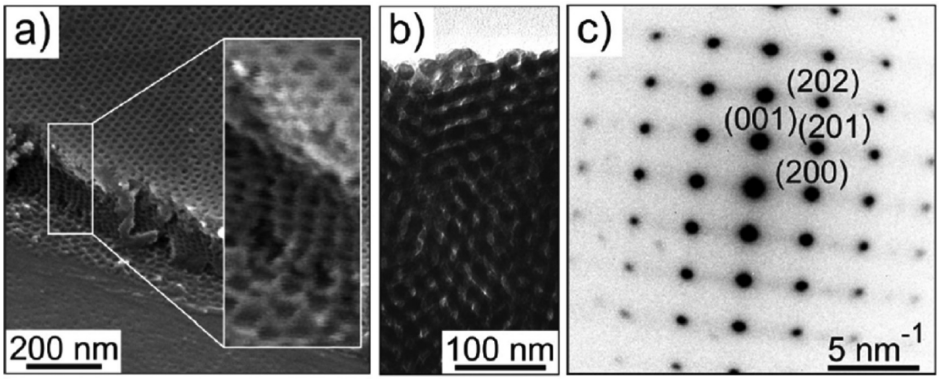

FIGURE 2. Morphology of KLE-templated *T*-Nb_2O_5 films with iso-oriented nanocrystalline pore walls. (a) Cross-sectional FESEM image of a razor-blade cut in a film held at a tilt of 45°. A higher-magnification image is shown in the inset of (a) confirming that the periodic structure observed on the top-surface persists throughout the film. (b) Bright-field TEM image. (c) Electron diffraction pattern obtained from the same sample shown in (b). The lattice-spacings correspond well with orthorhombic Nb_2O_5 (*T*-phase). (Adapted from ref 12. Copyright 2010 American Chemical Society.)

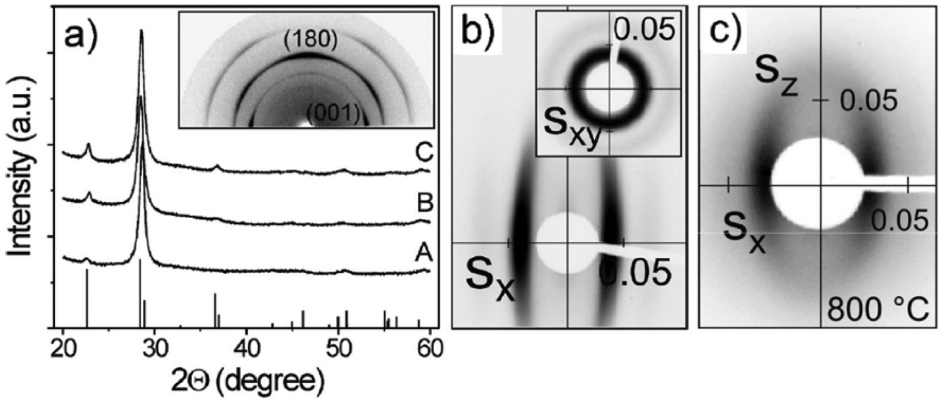

FIGURE 3. (a) 1D-WAXD data obtained on KLE-templated *T*-Nb_2O_5 (A), *L*-Ta_2O_5 (B), and $TaNbO_5$ (C) films. The stick pattern shows orthorhombic *T*-Nb_2O_5 according to JCPDS reference card #30-0873. A typical 2D-WAXD pattern for mesoporous *T*-Nb_2O_5 is shown in the inset of (a). (b) 2D-SAXS data obtained on cubic mesoporous Nb_2O_5 collected at angles of incidence $\beta = 10°$ and 90° (inset). (c) 2D-SAXS pattern of KLE22-templated nanocrystal-based cubic mesoporous TiO_2 film acquired at an angle of incidence $\beta = 7°$. (b, c) Scattering vector, *s*, components are given in 1/nm. (Adapted from refs 9 and 12. Copyright 2009 and 2010 American Chemical Society.)

crystallized at 600 °C. The film is macroscopically homogeneous with a well-ordered cubic network of open pores averaging 13−15 nm in diameter. The film was templated with poly(ethylene-*co*-butylene)-*b*-poly(ethylene oxide), a DBCP referred to as KLE. A unique property of these large DBCPs, when compared to surfactants and pluronics, is their ability to produce materials with thicker pore walls. During heating of a film with thick walls, crystallization can nucleate with a domain that has a critical size smaller than the pore wall. Nucleation and grain-growth can then both occur within the oxide wall, leading to a highly ordered mesoporous, yet crystalline structure.

In agreement with these ideas, most crystalline, polymer-templated mesoporous materials contain randomly oriented domains with diameters similar to or slightly larger than the average wall thickness. Nanoporous niobia, however, shows unique crystallization behavior that may positively influence its electrochemical performance. In Figure 2c, an electron diffraction pattern from a KLE-templated Nb_2O_5 film shows the presence of diffraction spots indicating that the crystalline domains are oriented relative to the substrate. The data specifically indicates oriented crystal growth along the [0*k*0] direction of the orthorhombic *T*-Nb_2O_5 nanodomains. To further characterize the crystal structure of these materials, wide-angle X-ray diffraction (WAXD) can be used. In Figure 3a, 1D-WAXD taken on mesoporous *T*-Nb_2O_5, *L*-Ta_2O_5, and $TaNbO_5$ films shows only one distinct peak, the (180) reflection, for all three samples indicating an iso-oriented crystallographic orientation with respect to the substrate. The inset shows a 2D-WAXD pattern which shows the other orthorhombic *T*-Nb_2O_5 peaks at off-normal angles. Similar oriented crystal growth has also been achieved in polymer-templated mesoporous α-MoO_3, which crystallizes into a 2D layered

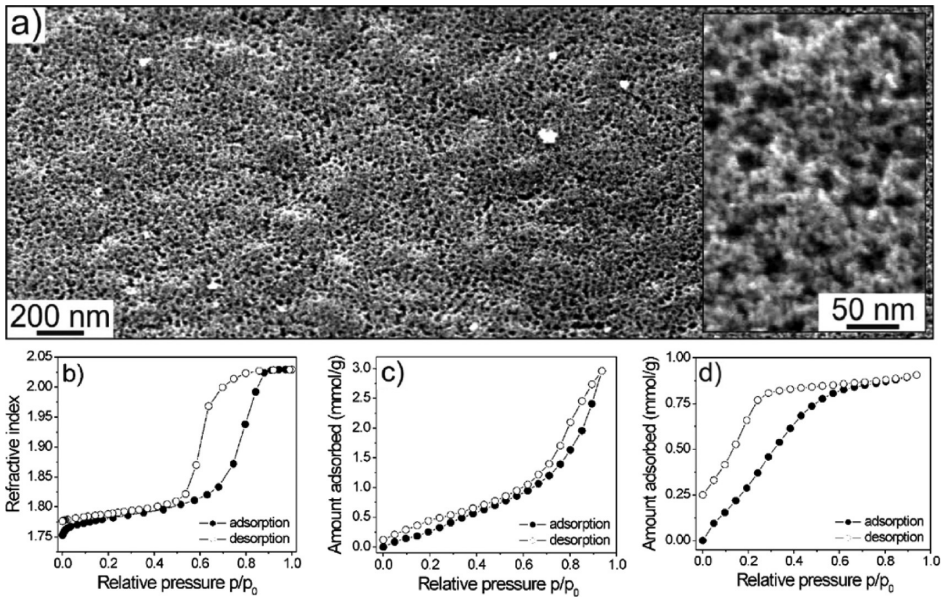

FIGURE 4. (a) Low-magnification top-view FESEM images of a KLE23-templated nanocrystal-based mesoporous TiO_2 film. The inset in (a) shows a high-magnification top-view FESEM image; the porosity is bimodal with 1−4 and 20−25 nm diameter pores. (b−d) Toluene adsorption−desorption isotherms for self-organized TiO_2 thin-films. (b) KLE22-templated sol−gel film, showing a standard isotherm for a sol−gel derived film with a monomodal pore structure. (c) KLE23-templated nanocrystal film with bimodal porosity. (d) Untemplated nanocrystal film with sub-4 nm pores that are formed by random nanocrystal aggregation. (Adapted from ref 9. Copyright 2009 American Chemical Society.)

structure with van der Waal gaps in between the stacked layers (Figure 6a). The interlayer gaps in these systems can be used for Li^+ intercalation. A more detailed discussion of the role of these oriented structures in Li^+ intercalation is given in section 5.

Another route to synthesizing crystalline, nanoporous films is to use preformed nanocrystals as building blocks (Scheme 1).[9,13,27−29] Templated nanocrystal-based materials show much higher surface areas than the sol−gel derived systems discussed above, and are thus an ideal way to build redox pseudocapacitance into a material. Figure 4a shows an example of a nanocrystal-based mesoporous TiO_2 architecture. The high magnification SEM image (inset) shows TiO_2 nanocrystals embedded in the pore walls. A detailed pore analysis on the nanocrystal-based TiO_2 system was obtained by toluene physisorption based on gravimetric measurements with a quartz crystal microbalance device or by ellipsometric porosimetry. Figure 4b−d shows typical adsorption−desorption isotherms for (b) templated sol−gel TiO_2, (c) templated nanocrystal-based TiO_2, and (d) untemplated TiO_2 nanocrystals. The main point to draw from these data is that the templated nanocrystal film exhibits a bimodal porosity with larger mesopores, left behind by the template, and smaller micropores, formed between the nanocrystals, leading to a substantial increase in surface area which can in turn produce an increase in pseudocapacitance.

For mesoporous films, the nanoscale structure can be examined by two-dimensional small-angle X-ray scattering (2D-SAXS). Figure 3b shows 2D-SAXS data obtained on a cubic mesoporous Nb_2O_5 film heated to 600 °C, and Figure 3c shows patterns for a nanocrystal-based TiO_2 film. The Nb_2O_5 film produces diffraction patterns with distinct in-plane maxima indexed to a body centered cubic (bcc) pore system with a (110) orientation relative to the plane of the substrate and a lattice parameter of 33−35 nm. The TiO_2 nanocrystal film, by contrast, produces a more diffuse ellipsoidal ring which is characteristic of a more disordered pore system with a characteristic length scale of 35 nm. Taken together, these synthetic routes and characterization methods allow us to produce redox-active materials with a diverse set of structures. Electrochemical analysis of these materials (described below) then lets us develop general design rules for fabricating polymer-templated mesoporous metal oxide electrode materials.

4. Quantifying Capacitive Properties

We have investigated the electrochemical behavior of mesoporous thin-films of TiO_2, CeO_2, MoO_3, and Nb_2O_5 in a nonaqueous Li^+ electrolyte with several techniques that use kinetic behavior to distinguish between surface and bulk charge storage. These materials can all intercalate Li^+, and therefore, careful analysis is needed to separate capacitive

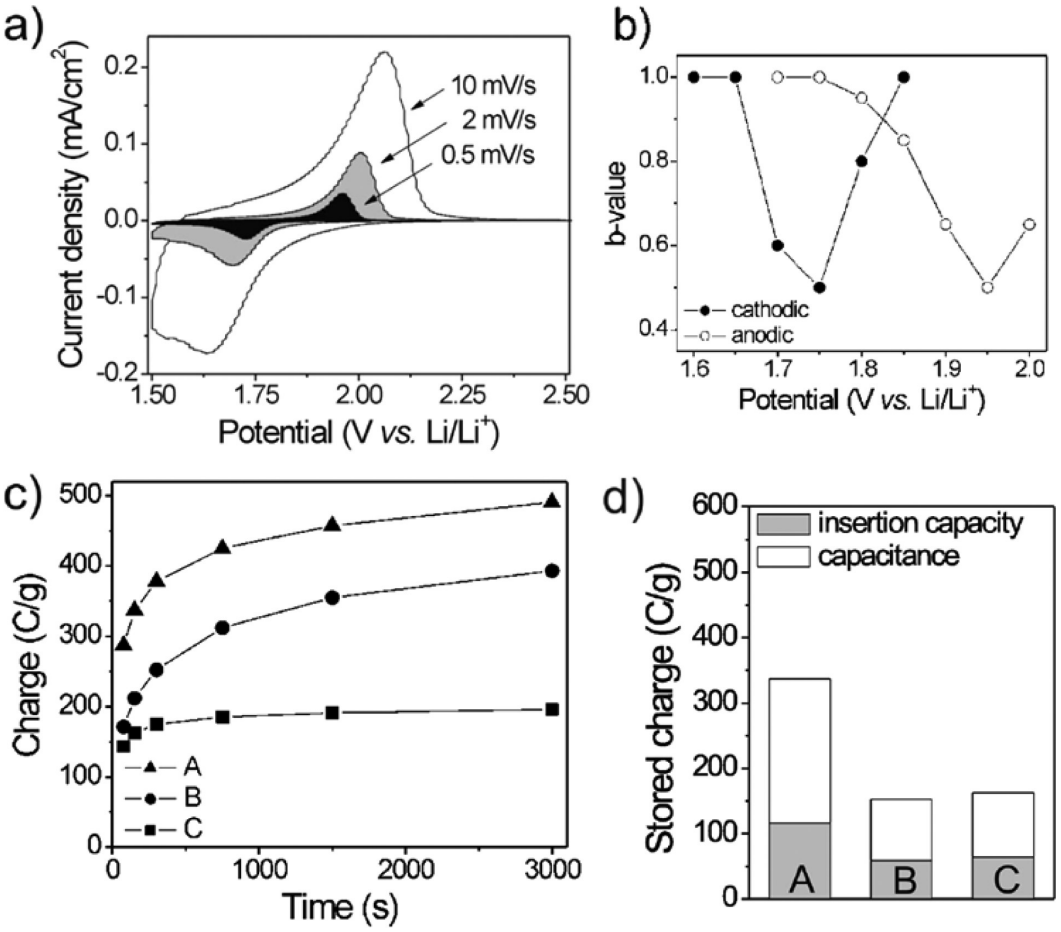

FIGURE 5. (a) Typical CV responses of KLE-templated nanocrystal-based TiO_2 films at various sweep rates. (b) Calculated *b*-values for a KLE-templated nanocrystal-based TiO_2 film as a function of potential for the cathodic (Li^+ insertion) and anodic sweep (Li^+ extraction). (c, d) Comparison of charging rates (c) and total stored charge at a sweep rate of 10 $mV \cdot s^{-1}$ (d) for various TiO_2 films. A and C refer to KLE-templated and untemplated nanocrystal films, while B refers to KLE-templated sol–gel films. (Adapted from ref 9. Copyright 2009 American Chemical Society.)

from diffusive contributions. Here, we describe three ways to do that. First, the current at a particular potential is kinetically separated into capacitive and diffusive contributions. Second, double-layer capacitance is directly measured by performing cyclic voltammetry in a bulky electrolyte. Finally, electrochemical impedance spectroscopy (EIS) at different potentials is used to analytically estimate pseudocapacitive and double-layer contributions.

4.1. Differentiating between Capacitance and Diffusion Currents. In a cyclic voltammetry experiment, the current is a function of the sweep rate and can generally be expressed as

$$i(V) = av^b$$

where *i* is the current, *V* is the potential, *v* is the sweep rate of the experiment (in $mV \cdot s^{-1}$), and *a* and *b* are adjustable constants. For the analysis, we assume that currents arising from bulk intercalation processes follow semi-infinite linear diffusion kinetics and therefore will vary as $v^{1/2}$. In contrast, currents resulting from surface charge storage processes will have a capacitive response and vary linearly with *v*. The *b*-value in the above equation is therefore an estimate of the type of charge storage occurring in the material: if *b* is 0.5, then the current is diffusion-controlled; if *b* is 1, then the current is capacitive.

For nanocrystal-templated mesoporous TiO_2, CV curves collected at scan rates from 10 to 0.5 $mV \cdot s^{-1}$, and *b*-values as a function of potential are shown in Figure 5a and b, respectively. The *b*-value at the peak potentials of 1.75 and 1.95 V (cathodic and anodic sweeps, respectively), is approximately 0.5 while away from the peaks, the *b*-value increases until it reaches ~1. This analysis demonstrates that while the peak potential currents are primarily due to diffusion processes, capacitive contribution dominates away from the peaks.

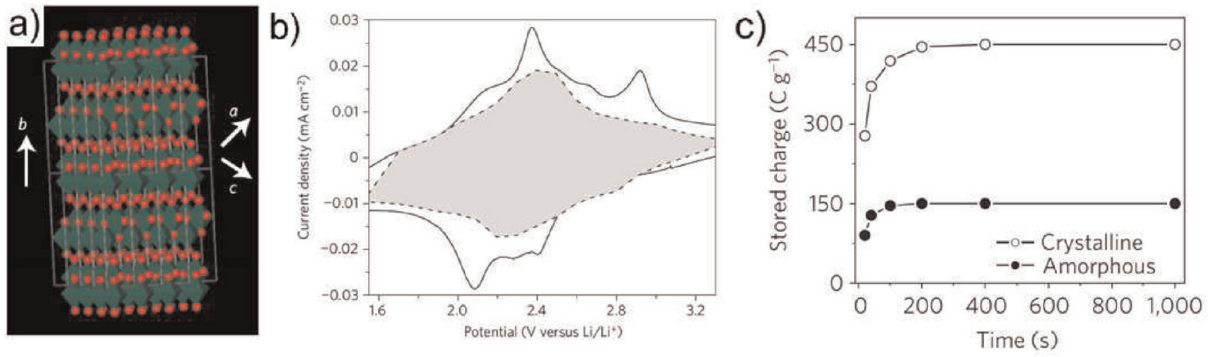

FIGURE 6. (a) Molybdite (α-MoO_3) unit cells showing the layer-like arrangement of molybdenum (green) and oxygen atoms (red). (b) CV at 0.1 $mV \cdot s^{-1}$ of mesoporous α-MoO_3: the pseudocapacitive contribution is shaded, as deduced from current analysis. (c) The capacitive contribution to the total stored charge plotted as function of charging time for a mesoporous amorphous MoO_3 film and a mesoporous α-MoO_3 film. The capacitive contribution for the mesoporous crystalline film is three times larger than the amorphous analogue. (Adapted from ref 10. Copyright Macmillan Publishers 2010.)

The current behavior can be described in a more precise manner by separating the diffusion and capacitive contributions at a particular potential, as proposed by Liu et al.:[30]

$$i(V) = k_1 v^{1/2} + k_2 v$$

Solving for k_1 and k_2 gives the capacitive and diffusion contributions to the current.

Figure 6b demonstrates this analysis applied to iso-oriented mesoporous α-MoO_3. The pseudocapacitive contribution (shaded-region) is characterized by broad peaks characteristic of surface-confined charge storage.[10] Such a response is unique to the mesoporous, iso-oriented architecture. From this curve, the charge storage due to capacitive processes is estimated and the results are compared at different sweep rates and charging times, as shown in Figure 6c for MoO_3.

4.2. Estimating Double-Layer Capacitance. Capacitive charge storage consists of contributions from both pseudocapacitive and double-layer effects. One way to estimate the amount of double-layer capacitance in a material that exhibits pseudocapacitance is to perform cyclic voltammetry with a bulky cation electrolyte, such as tetrabutylammonium (TBA^+) perchlorate.[12] Figure 7 demonstrates the CV response of mesoporous *T*-Nb_2O_5 in both Li^+ and TBA^+ electrolytes. Clearly, in the bulkier electrolyte, the overall charge storage is smaller. This result indicates that only ~10% of the charge storage in *T*-Nb_2O_5 is due to double-layer capacitance. The rest is due to faradaic redox processes.

Another way to separate the double-layer and pseudocapacitance is to use analytical modeling based on EIS. An example of this technique applied to mesoporous CeO_2 is

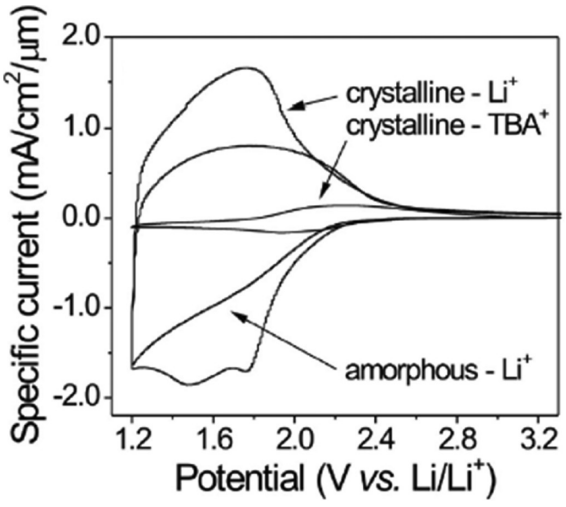

FIGURE 7. CV ($v = 10$ $mV \cdot s^{-1}$) of crystalline and amorphous mesoporous *T*-Nb_2O_5 in Li^+ and TBA^+ nonaqueous electrolytes. Here TBA^+ is used to estimate the double-layer capacitance. The results demonstrate the small contribution of double-layer capacitance to the overall charge storage (Adapted from ref 12. Copyright 2010 American Chemical Society).

shown in Figure 8. A simple circuit is used to model the response at different points during lithiation, as shown in Figure 8a. Upon lithium insertion into the CeO_2 film, the electronic conductivity increases and charge is accumulated through capacitive processes. The double-layer capacitance is independent of the potential, whereas the pseudocapacitance does depend on the applied voltage (Figure 8c). EIS can thus be used to corroborate the role of pseudocapacitance in charge storage of metal oxide films.

4.3. Cycle-Life. An important question that has yet to be addressed with mesoporous materials is their lifetime and cyclability. Lifetime behavior of pseudocapacitor materials has received only limited study, but early results

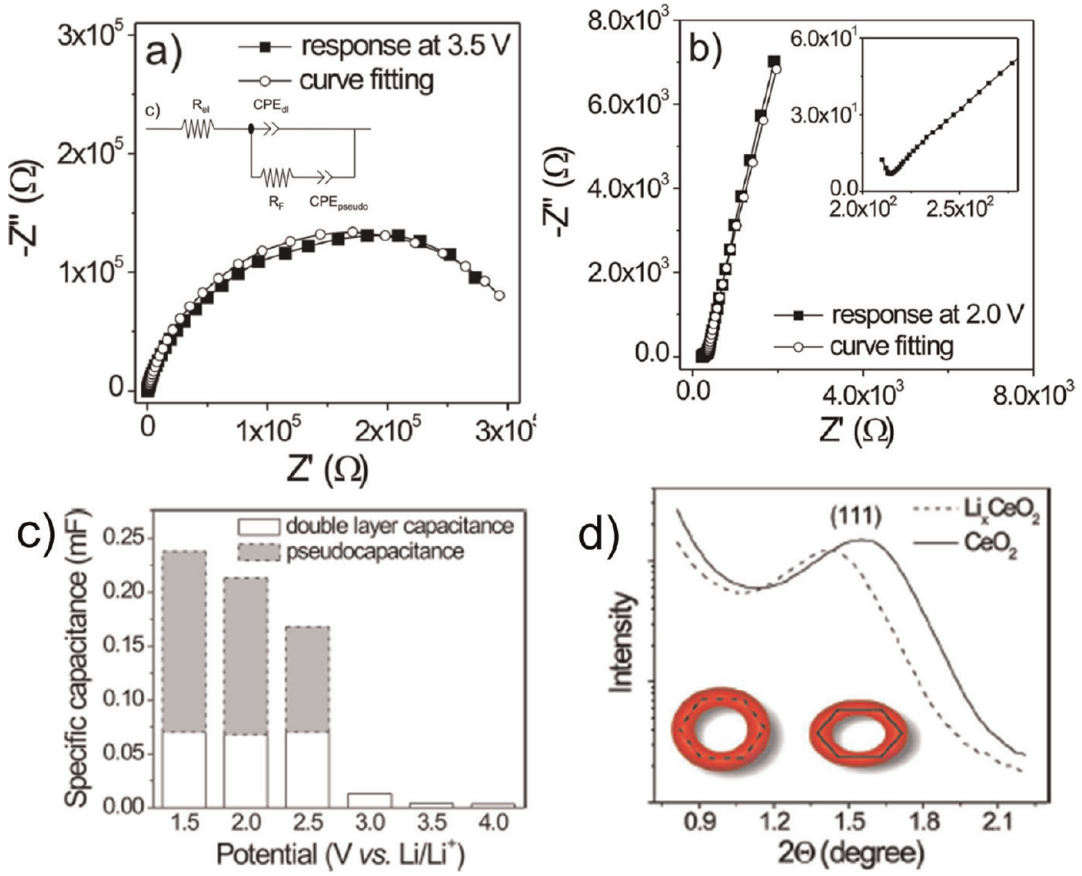

FIGURE 8. Electrochemical studies of mesoporous crystalline CeO_2. (a–c) Use of EIS to separate pseudocapacitance and double-layer capacitance: (a) impedance response at 3.5 V and (b) after lithiation to 2 V. The proposed circuit model is shown as an inset to (a). (c) Results of the fitting analysis demonstrate that pseudocapacitance accounts for a significant fraction of the charge storage. (d) Low-angle XRD indicates that the pores flex in response to the volume change upon lithiation. (Adapted from ref 11. Copyright 2010 American Chemical Society.)

are promising. Asymmetric capacitors that incorporate one pseudocapacitive electrode show stable device operation in excess of 8000 cycles,[4] well beyond the performance of batteries. We expect mesoporous materials to perform similarly.

5. Design Rules for Pseudocapacitor Electrodes

The advantage of working with thin-films is it allows us to investigate the fundamental charge storage properties of mesoporous materials. This, along with the work of others on porous electrodes, has led to a better understanding of what type of architectures can be used to optimize pseudocapacitive charge storage. The attributes required for an effective pseudocapacitive architecture include high surface area, interconnected porosity, mechanical flexibility, nanodimensionality, and effective electron transport. We illustrate these design principles through examples from our work on mesoporous transition metal oxides.

5.1. Small Nanosized Building Units for High Surface Area. Perhaps the most obvious requirement for pseudocapacitive charge storage is to utilize a high surface area material. An effective electrode architecture should maintain the high surface area of nanocrystals without burying them in conductive additives or binders. Polymer-templated nanocrystals with bimodal porosity (Figure 4) demonstrate the dramatic effect of increased surface area on the charge storage properties of anatase TiO_2. Figure 5c and d compares the charge storage behavior observed for (A) polymer-templated nanocrystal films, (B) polymer-templated sol–gel films, and (C) untemplated nanocrystal films. The pseudocapacitive contribution to charge storage is nearly 65% of the total stored charge for the templated nanocrystal film at faster sweep rates. In addition, the data suggests the total amount of stored charge and charging/discharging rates improve significantly for the templated nanocrystals. These results can be attributed to the bimodal porosity, with larger mesopores that allow for electrolyte diffusion, and smaller

micropores that expose many redox active sites on the surface of the TiO_2 to the electrolyte.

5.2. Mesoporosity to Facilitate Solvent Diffusion. The work on templated porous TiO_2 films also underscores the advantage of creating mesoporous architectures with three-dimensionally interconnected porosity (Figure 5c). The significance becomes apparent from the larger stored charge in the templated nanocrystal film. The data suggest that the electrochemical charge/discharge properties are enhanced by (1) minimizing the solid-state diffusion path lengths and (2) facilitating ion/solvent transport to the active sites.

It can also be inferred from the data that in order to obtain fast solvent transport pathways, a minimum pore size is needed. This is evident by comparing the templated and untemplated nanocrystal-based films. In the latter case, the pore spaces between the nanocrystals (micropores) are too small, hindering ion/solvent diffusion. The combination of open mesopores with nanocrystal building blocks thus provides a general synthetic route for improving both the surface area and the diffusion of electrolyte through the electrode.

5.3. Flexible Architectures to Facilitate Volume Expansion. One unique aspect of mesoporous films is that the ordered porosity, nanodimensions, and in some cases, iso-orientation, allow the structure to be flexible. This feature may be particularly beneficial for systems that exhibit intercalation pseudocapacitance. As ions incorporate into the layers and tunnels of such materials, size constraints and electrostatic repulsions result in lattice expansion. In bulk materials, high-rates of lithiation produce uneven lithium distribution in the material, leading to significant stress and eventually fracture.[31] In EC applications, the charging rates are much higher than in batteries; as the physical mechanism of intercalation pseudocapacitance is similar to that of lithium-ion batteries, the stresses can be very high. Despite this fact, materials like mesoporous *T*-Nb_2O_5 can be charged and discharged reversibly within seconds.

The ordered porosity and nanodimensions of mesoporous films can be modeled as a nanotruss architecture. The effects of these nanotrusses were examined using 1D-SAXS experiments, carried out on mesoporous crystalline CeO_2 to see how the nanoscale repeat distance changes with cycling (Figure 8d).[11] These experiments demonstrated that after fully lithiating the material for 2 h, the film expanded by about 10% normal to the substrate, as measured by changes in the pore-to-pore distance. The low angle diffraction peak does not broaden upon Li^+ intercalation, indicating that the framework can easily flex to accommodate the volume expansion associated with insertion.

In addition to the nanotruss architecture of all these sol−gel mesoporous films, α-MoO_3 and *T*-Nb_2O_5 preferentially crystallize in an iso-oriented manner, with the preferred intercalation planes parallel to the substrate.[10,12] The advantage of iso-orientation in such layered and tunnel materials is that expansion during lithiation is all normal to the substrate, which can readily be relaxed by pore flexing.

5.4. Nanosized Domains. Thus far we have established that as the dimensions of electroactive materials approach the nanoscale, the total surface area and therefore the availability of redox active sites in the material increases substantially. We have also demonstrated how maintaining an interconnected open mesoporous architecture leads to facile diffusion of ions/electrolyte to the electrochemically active sites. We now return to the concept of "iso-oriented" crystalline domains. Figure 6c compares the capacitive charge storage as a function of charging time for an iso-oriented mesoporous α-MoO_3 film with a mesoporous amorphous MoO_3 film.[10] The crystalline film shows faster charging and higher capacity than the amorphous film. While surface-confined redox pseudocapacitance should occur in both types of films, the capacitive contribution is significantly higher for the crystalline film (almost 70%), compared to the amorphous film (only 35%). Therefore, in this system, it appears that intercalation pseudocapacitance associated with the fast insertion of Li^+ into the van der Waal gaps of the MoO_3 occurs on the same time scale as redox pseudocapacitance. The unique combination of a high surface area, open porosity, and the nearly perfect crystallographic alignment of the intercalation layers provide very short diffusion path lengths that allow facile insertion into layers without compromising kinetics. Similar intercalation pseudocapacitance is observed in mesoporous Nb_2O_5.[12]

6. Conclusions

The significance of the work reviewed here is to outline systematic ways to improve the electrochemical properties of capacitive storage devices through careful design of the electrode architecture. Enhanced device performance is realized through integration of one or more of the following design rules into electrode architecture: assembling small nanosized building blocks to increase surface area, maintaining an interconnected open mesoporosity to facilitate solvent diffusion, flexibility in the structure to facilitate volume expansion during ion insertion, well-defined nanodimensional domains, possibly with oriented crystalline layers to facilitate ion intercalation into the lattice, and creation of effective electron transport pathways. The latter

is especially important because good electronic conductivity is essential for creating thicker films that can store more energy per area and volume. Several groups have already demonstrated the significant benefits of combining pseudocapacitive materials with good electron conductors,[20] but these architectures usually contain a significant amount of inactive material. The goal for the next generation of mesoporous supercapacitors is to scale these optimized architectures to bulk form. Through exploration of new electrode architectures, the advancement of electrochemical capacitors to the forefront of next-generation energy storage devices can become a reality.

This work was supported by the Center for Molecularly Engineered Energy Materials, an Energy Frontier Research Center funded by the DOE Office of Basic Energy Sciences (DE-SC001342).

BIOGRAPHICAL INFORMATION

Iris E. Rauda received her B.S. and M.S. degrees from California State University Los Angeles in 2003 and 2006, respectively. She received a Ph.D. in Chemistry at UCLA under the supervision of Professor Sarah Tolbert in 2012. Her thesis research focused on solution-phase routes to nanoporous and nanostructured materials for applications in clean energy.

Veronica Augustyn received her B.S. in Materials Science & Engineering from the University of Arizona in 2007. She is currently pursuing her Ph.D. under Professor Bruce Dunn at UCLA. Her thesis research focuses on the characterization and analysis of novel energy storage materials.

Bruce Dunn is the Nippon Sheet Glass Professor of Materials Science and Engineering at UCLA. Prior to joining UCLA in 1981, he was a staff scientist at the General Electric Research Laboratory. His research interests focus on the synthesis of inorganic and organic/inorganic materials, and the design of their electrochemical, optical, and biorecognition properties. His current programs in electrochemistry include creating pseudocapacitive materials and the fabrication of three-dimensional batteries. Professor Dunn has received a number of honors including a Fulbright research fellowship, invited professorships at the University of Paris and the University of Bordeaux, and two awards from the Department of Energy for Outstanding Research in Materials Science. He is a Fellow of the American Ceramic Society and the Materials Research Society.

Sarah H. Tolbert is a professor in the Departments of Chemistry and Biochemistry and Materials Science and Engineering at UCLA. Prior to joining the faculty at UCLA, she received a B.S. from Yale University, a Ph.D. from U.C. Berkeley, and was an NSF postdoctoral fellow at U.C. Santa Barbara. Her research focuses on controlling nanometer-scale architecture in solution-processed nanomaterials to generate unique optical, electronic, magnetic, structural, and electrochemical properties. She also leads a program aimed at bringing nanoconcepts to high school students in the greater LA area. Professor Tolbert is the recipient of a number of awards including the Office of Naval Research Young Investigator Award, an NSF CAREER Award, a Beckman Young Investigator Award, and a Sloan Foundation Research Fellowship.

FOOTNOTES

*E-mail: tolbert@chem.ucla.edu (S.H.T.); bdunn@ucla.edu (B.D.).
The authors declare no competing financial interest.
‖I.E.R. and V.A. contributed equally to this work.

REFERENCES

1 *Basic Research Needs for Electrical Energy Storage*; Office of Basic Sciences, U.S. Department of Energy: Washington, DC, April 2007.

2 Simon, P.; Gogotsi, Y. Materials for Electrochemical Capacitors. *Nat. Mater.* **2008**, *7*, 845–854.

3 Miller, J. R.; Simon, P. Electrochemical Capacitors for Energy Management. *Science* **2008**, *321*, 651–652.

4 Naoi, K. Nanohybrid Capacitor: The Next Generation Electrochemical Capacitors. *Fuel Cells* **2010**, *10*, 825–833.

5 Conway, B. E. *Electrochemical Supercapacitors: Scientific Fundamentals and Technological Applications*; Kluwer Academic: New York, 1999.

6 Largeot, C.; Portet, C.; Chmiola, J.; Taberna, P.-L.; Gogotsi, Y.; Simon, P. Relation between the Ion Size and Pore Size for an Electric Double-Layer Capacitor. *J. Am. Chem. Soc.* **2008**, *130*, 2730–2731.

7 Bazant, M. Z.; Storey, B. D.; Kornyshev, A. A. Double Layer in Ionic Liquids: Overscreening versus Crowding. *Phys. Rev. Lett.* **2011**, *106*, 046102(1−4).

8 Conway, B. E.; Pell, W. G. Double-layer and Pseudocapacitance Types of Electrochemical Capacitors and their Applications to the Development of Hybrid Devices. *J. Solid State Electrochem.* **2003**, *7*, 637–644.

9 Brezesinski, T.; Wang, J.; Polleux, J.; Dunn, B.; Tolbert, S. H. Templated Nanocrystal-Based Porous TiO_2 Films for Next-Generation Electrochemical Capacitors. *J. Am. Chem. Soc.* **2009**, *131*, 1802–1809.

10 Brezesinski, T.; Wang, J.; Tolbert, S. H.; Dunn, B. Ordered Mesoporous α-MoO_3 with Iso-Oriented Nanocrystalline Walls for Thin-Film Pseudocapacitors. *Nat. Mater.* **2010**, *9*, 146–151.

11 Brezesinski, T.; Wang, J.; Senter, R.; Brezesinski, K.; Dunn, B.; Tolbert, S. H. On the Correlation between Mechanical Flexibility, Nanoscale Structure, and Charge Storage in Periodic Mesoporous CeO_2 Thin Films. *ACS Nano* **2010**, *4*, 967–977.

12 Brezesinski, K.; Wang, J.; Haetge, J.; Reitz, C.; Steinmueller, S. O.; Tolbert, S. H.; Smarsly, B. M.; Dunn, B.; Brezesinski, T. Pseudocapacitive Contributions to Charge Storage in Highly Ordered Mesoporous Group V Transition Metal Oxides with Iso-Oriented Layered Nanocrystalline Domains. *J. Am. Chem. Soc.* **2010**, *132*, 6982–6990.

13 Rauda, I. E.; Buonsanti, R.; Saldarriaga-Lopez, L. C.; Benjauthrit, K.; Schelhas, L. T.; Stefik, M.; Augustyn, V.; Ko, J.; Dunn, B.; Wiesner, U.; Milliron, D. J.; Tolbert, S. H. General Method for the Synthesis of Hierarchical Nanocrystal-Based Mesoporous Materials. *ACS Nano* **2012**, *6*, 6386–6399.

14 Brezesinski, K.; Haetge, J.; Wang, J.; Mascotto, S.; Reitz, C.; Rein, A.; Tolbert, S. H.; Perlich, J.; Dunn, B.; Brezesinski, T. Ordered Mesoporous α-Fe_2O_3 (Hematite) Thin-Film Electrodes for Application in High Rate Rechargeable Lithium Batteries. *Small* **2011**, *7*, 407–414.

15 Tiwari, J. N.; Tiwari, R. N.; Kim, K. S. Zero-Dimensional, One-Dimensional, Two-Dimensional and Three-Dimensional Nanostructured Materials for Advanced Electrochemical Energy Devices. *Prog. Mater. Sci.* **2012**, *57*, 724–803 and references therein.

16 Ren, Y.; Ma, Z.; Bruce, P. G. Ordered Mesoporous Metal Oxides: Synthesis and Applications. *Chem. Soc. Rev.* **2012**, *41*, 4909–4927 and references therein.

17 Cheng, F.; Tao, Z.; Liang, J.; Chen, J. Template-Directed Materials for Rechargeable Lithium-Ion Batteries. *Chem. Mater.* **2008**, *20*, 667–681 and references therein.

18 Dong, W.; Rolison, D. R.; Dunn, B. Electrochemical Properties of High Surface Area Vanadium Oxide Aerogels. *Electrochem. Solid State Lett.* **2000**, *3*, 457–459.

19 Zhang, H.; Yu, X.; Braun, P. V. Three-Dimensional Bicontinuous Ultrafast-Charge and - Discharge Bulk Battery Electrodes. *Nat. Nanotechnol.* **2011**, *6*, 277–281.

20 Liu, R.; Duay, J.; Lee, S. B. Heterogeneous Nanostructured Electrode Materials for Electrochemical Energy Storage. *Chem. Commun.* **2011**, *47*, 1384–1404 and references therein.

21 Gogotsi, Y.; Simon, P. True Performance Metrics in Electrochemical Energy Storage. *Science* **2011**, *334*, 917–918.

22 Lokhande, C. D.; Dubal, D. P.; Joo, O.-S. Metal Oxide Thin Film Based Supercapacitors. *Curr. Appl. Phys.* **2011**, *11*, 255–270 and references therein.

23 Kresge, C. T.; Leonowicz, M. E.; Roth, W. J.; Vartuli, J. C.; Beck, J. S. Ordered Mesoporous Molecular Sieves Synthesized by a Liquid-Crystal Template Mechanism. *Nature* **1992**, *359*, 710–712.

24 Zhao, D. Y.; Feng, J. L.; Huo, Q. S.; Melosh, N.; Fredrickson, G. H.; Chmelka, B. F.; Stucky, G. D. Triblock Copolymer Synthesis of Mesoporous Silica with Periodic 50 to 300 Angstrom Pores. *Science* **1998**, *279*, 548–552.

25 Templin, M.; Franck, A.; Du Chesne, A.; Leist, H.; Zhang, Y.; Ulrich, R.; Schadler, V.; Wiesner, U. Organically Modified Aluminosilicate Mesostructures from Block Copolymer Phases. *Science* **1997**, *278*, 1795–1798.

26 Lu, Y. F.; Ganguli, R.; Drewien, C. A.; Anderson, M. T.; Brinker, C. J.; Gong, W. L.; Guo, Y. X.; Soyez, H.; Dunn, B.; Huang, M. H.; Zink, J. I. Continuous Formation of Supported Cubic and Hexagonal Mesoporous Films by Sol Gel Dip-Coating. *Nature* **1997**, *389*, 364–368.

27 Warren, S. C.; Messina, L. C.; Slaughter, L. S.; Kamperman, M.; Zhou, Q.; Gruner, S. M.; DiSalvo, F. J.; Wiesner, U. Ordered Mesoporous Materials from Metal Nanoparticle−Block Copolymer Self-Assembly. *Science* **2008**, *320*, 1748–1752.

28 Deshpande, A. S.; Pinna, N.; Smarsly, B.; Antonietti, M.; Niederberger, M. Controlled Assembly of Preformed Ceria Nanocrystals into Highly Ordered 3D Nanostructures. *Small* **2005**, *1*, 313–316.

29 Ba, J.; Polleux, J.; Antonietti, M.; Niederberger, M. Non-aqueous Synthesis of Tin Oxide Nanocrystals and Their Assembly into Ordered Porous Mesostructures. *Adv. Mater.* **2005**, *17*, 2509–2512.

30 Liu, T.-C.; Pell, W. G.; Conway, B. E.; Roberson, S. L. Behavior of Molybdenium Nitrides as Materials for Electrochemical Capacitors. *J. Electrochem. Soc.* **1998**, *145*, 1882–1888.

31 Zhao, K.; Pharr, M.; Vlassak, J. J.; Suo, Z. Fracture of Electrodes in Lithium-Ion Batteries caused by Fast Charging. *J. Appl. Phys.* **2010**, *108*, 073517-(1−6).